Proceedings of the ASME 2023 18th International
Manufacturing Science and Engineering Conference
MSEC2023
June 12-16, 2023, New Brunswick, NJ, USA

MSEC2023-105134

MODEL CALIBRATION IN INKJET PRINTING PROCESS

Christian Zuniga-Navarrete[1], Chi Zhou[2], Hongyue Sun[2], Luis Javier Segura[1,*]

[1]Department of Industrial Engineering, University of Louisville, Louisville, KY 40292, United States
[2]Department of Industrial and Systems Engineering, University at Buffalo, SUNY Buffalo, NY 14260, United States

ABSTRACT

Inkjet printing (IJP) is an additive manufacturing process capable to produce intricate functional structures. The IJP process performance and the quality of the printed parts are considerably affected by the deposited droplets' volume. Obtaining consistent droplets volume during the process is difficult to achieve because the droplets are prone to variations due to various material properties, process parameters, and environmental conditions. Experimental (i.e., IJP setup observations) and computational (i.e., computational fluid dynamics (CFD)) analysis are used to study the droplets variability; however, they are expensive and computationally inefficient, respectively. The objective of this paper is to propose a framework that can perform fast and accurate droplet volume predictions for unseen IJP driving voltage regimes. A two-step approach is adopted: (1) an emulator is constructed from the physics-based droplet volume simulations to overcome the computational complexity and (2) the emulator is calibrated by incorporating the experimental IJP observations. In particular, a scaled Gaussian stochastic process (s-GaSP) is deployed for the emulation and calibration. The resulting surrogate model is able to rapidly and accurately predict the IJP droplets volume. The proposed methodology is demonstrated by calibrating the simulated data (i.e., CFD droplet simulations) emulator with experimental data from two distinct materials, namely glycerol and isopropyl alcohol.

Keywords: Inkjet Printing Process, Additive Manufacturing, Model Calibration, Gaussian Stochastic Process

1. INTRODUCTION

Additive manufacturing (AM) is an advanced manufacturing technique that has undergone extensive development since it emerged in 1987 [1]. Moreover, some AM techniques (e.g., material extrusion, inkjet printing, etc.) have been extensively applied since they have overcome the limitations of traditional manufacturing techniques (e.g., material waste, geometrics design, etc.); hence, expanding the AM applications spectrum. However, AM still suffers from defects, such as dimensional inconsistency and stair-stepping effect, as a result of the layered structure, which affects the quality of the printed parts. Here, multiple efforts have been proposed to ameliorate the AM deffects [2–5]. Among the different AM technologies, the inkjet printing (IJP) process has attracted attention in various application fields, such as health, electronics, energy, biomedical areas, etc. [6–9], due to its capability to produce complicated features with high-resolution, high-flexibility, and low-cost [10].

Two IJP-based methods have been widely explored, namely continuous and drop-on-demand (DOD) IJP processes [11]. The DOD method can achieve the highest resolution at a low production cost [12]; and a suitable technique for droplet generation in DOD fashion is the piezoelectric technology. Fig. 1 shows a scheme of the piezoelectric IJP process. Droplets are generated by the action of a piezoelectric transducer [13]. In response to the applied voltage, the piezoelectric movement contracts the volume in the nozzle and this causes the droplet ejection and deposition onto a substrate [14]. The droplet behavior is sensitive to material properties (e.g., surface tension, viscosity, and density) [15], process parameters (e.g., contact angle, substrate temperature) [16, 17], and environmental conditions (e.g., humidity, temperature) [18]; hence, obtaining consistent droplet features, such as droplet size, shape, and volume, for optimal product quality is challenging [19].

A variety of studies have been devoted to investigating droplet features, such as formation [20], evolution [21], and volume [22]; however, understanding their governing mechanism is burdensome. Empirical methods have attempted to improve process quality and reliability by collecting and analyzing *in-situ* process data. Vision systems (e.g., borescope, charged-couple device (CCD) camera, etc.) have been widely used since droplet features can be obtained from their images [23]. For example, an imaging system was used to analyze droplet formation in a IJP process [24]. Wu et al. [25] developed an approach to predict droplet velocity and volume from process images. Although

*Corresponding author: ljsegu01@louisville.edu
Documentation for `asmeconf.cls`: Version 1.32, February 21, 2023.

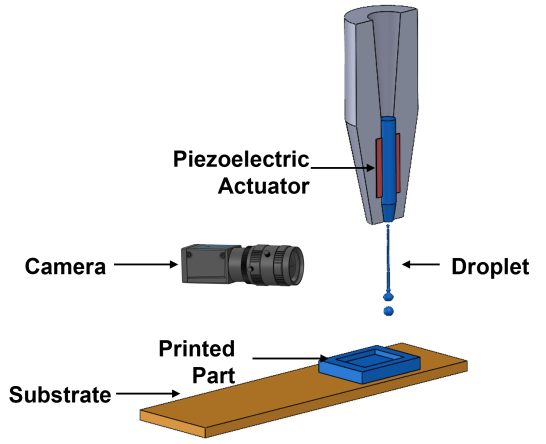

FIGURE 1: Piezoelectric IJP Process Scheme.

empirical methods can help to predict and control the droplet features in the IJP process, they generate material waste and can be costly due to large amount of data requirements. Additionally, the empirical methods do not consider the governing physics of the droplets [26], which may harm the accuracy of the analysis.

Physics-based methods have been explored to study and optimize the IJP process. For instance, several researchers used computational fluid dynamics (CFD) to study the different IJP droplet features (e.g., volume) under the influence of different material properties (e.g., viscosity) [27] and process parameters (e.g., driving voltage) [16]. Wu et al. [28] analyzed the droplet behavior based on a solution algorithm scheme coupled with the volume of fluid and continuum surface force models. Important progress in IJP process understanding has been achieved; however, physics-based models (e.g., CFD) heavily rely on assumptions, such as axisymmetric droplets and Newtonian fluids, which may not accurately reflect the reality and are computationally expensive [29]. This prevents researchers from extensive material and process parameters exploration.

Model emulation and calibration have been explored to address the computational efficiency and accuracy limitations from computer models (e.g., physics-based models), respectively. It is paramount to systematically integrate experimental observations (i.e., IJP droplet images) and simulated data (i.e., IJP droplet CFD images) to enhance statistical models (i.e., emulators) efficiency and accuracy so that a wide range of material and process parameters can be explored. In particular, experimental observations are required to obtain important accuracy improvement after model calibration [30]. For instance, Tuo et al. [31] proposed an L_2 calibration framework for imperfect computer models. However, the majority of calibration approaches require large experimental observations [32] to estimate unknown parameters (e.g., density, viscosity, etc.) for specific applications [30] and the model parameters may be unidentifiable due to poor experimental data fit.

The objective of this paper is to build a surrogate modeling framework that performs fast and accurate droplet volume predictions on the IJP process. An emulator is constructed from the simulated data and calibrated with the experimental data of IJP droplets. This is achieved via implementing a scaled Gaussian stochastic process (s-GaSP) for computer model calibration and prediction, proposed in [32]. Specifically, the s-GaSP models the discrepancy between the computer model and experimental data with a Gaussian stochastic process constrained to a scaling space [32]. The proposed framework is able to: (1) handle limited experimental observations (i.e., IJP droplets volume) for computer model calibration, (2) reduce the high-computationally burden of physics-based models, and (3) increase prediction accuracy to better reflect reality.

As will be demonstrated in the Case Study section, the proposed framework is able to accurately and rapidly predict the droplet volume in the IJP process for unobserved driving voltage regimes. The accuracy of the proposed framework is evaluated by computing the testing normalize root mean square error (NRMSE). The results showed that the proposed framework has high accuracy and efficiency. This framework can be applied to other processes, such as electrospinning and electrohidrodynamics IJP.

The paper is structured as follows. Section 2 briefly discusses related studies. The proposed framework will be described in Section 3. Section 4 will show the experimental results. Finally, Section 5 will conclude the paper and discuss future work.

2. LITERATURE REVIEW

2.1 Process Improvements in IJP

The IJP process has shown to be an effective technique to produce scalable, efficient, and low-cost parts [33, 34]. Moreover, the IJP process is capable to use a variety of materials, such as carbon nanotubes, metallic nanoparticles, graphene, biopolymers, among others [35, 36]. Hence, IJP has become an increasingly attractive option for the production of parts for a wide variety of applications (e.g., electronics, biomedical, and pharmaceutical fields). However, controlling the uniformity of droplet features (e.g., size, volume) is challenging, which affects the quality of the produced parts. Thus, experimental, data-driven, and physics-based modeling methods have been realized in order to ensure the droplet's features consistency [22].

Experimental approaches have been widely explored in the IJP process. Particular attention was paid to materials and process parameters to improving the IJP process performance. Cao et al. [22] developed a method to reveal the effect of printing parameters on the drop volume uniformity. Similarly, Laurila et al. [26] analyzed printing parameter effects on Ag-nanoparticle ink droplet size. Zhang et al. [37] showed the variation of the satellites' volume of the droplets maintaining the nozzle size. See other similar studies in [38, 39]. Although the experimental methods have shown the impact of the parameters in the IJP process, they do not consider the governing physics of the IJP process.

Furthermore, data-driven models have been applied to predict and control the IJP process. Generally, these methods have integrated vision systems and advanced computational algorithms to generate the model. For instance, Huang et al. [21] implemented an unsupervised learning method by deploying a deep recurrent neural network to study the droplet jetting behavior based on IJP process video data. Wu et al. [25] introduced an ensemble learning algorithm to predict droplet velocity and vol-

ume during IJP process. Ball et al. [40] developed a framework based on neural network algorithms to predict the ink droplets' diameter. See others in [41, 42]. Although data-driven models have been beneficial to improve the IJP processes, they require a large amount of data to perform well.

Physics-based modeling approaches have been developed to represent and optimize the IJP process. In particular, IJP droplet ejection, formation, and impingement have been mainly explored [21, 41]. Ramakrishnan et al. [43] analyzed the droplet formation in the ceramic IJP process by solving the mass and momentum conservation equations via commercial CFD-ACE+ software. Park et al. [44] simulated the forming of uniform inkjet-printed quantum dots, where the Navier-Stokes (NS) equations are solved to reduce the coffee ring effect. See also [45, 46]. These models have shown good performance; however, they rely on assumptions, i.e., Newtonian fluid, which may deplete their accuracy.

2.2 Model Calibration Approaches

Physics-based models (i.e., CFD) have demonstrated good performance at encoding complex behaviors in the IJP process [47]. However, they are computationally expensive, which prevents researchers from exploring a large variety of material and process parameters. To partially mitigate this limitation, model emulation has been explored since it can deliver fast predictions; hence, enabling the exploration of a wide range of material and process parameters in short periods of time [48]. Nevertheless, emulators may be inaccurate since they rely on physics-based approximations (i.e., IJP CFD droplet simulations in our case), which are already estimations of the IJP physical observations. In addition, for specific applications, the values of necessary parameters (e.g., density, viscosity, and surface tension) may be unknown; therefore, experimental observations of the system (i.e., IJP process droplets) are used to learn the unknown parameters [30]. Model calibration is achieved by fitting the emulator's parameters to the experimental observations; consequently, model accuracy is considerably increased to better reflect reality.

Several calibration techniques have been implemented to improve computer models performance. Statistical methods have been widely explored. For instance, Tuo et al. [31] develop a calibration framework for limited data processes. Sargsyan et al. [49] deployed a Bayesian statistical method to calibrate a chemical model. See also [50, 51]. In addition, neural network-based approaches have been also studied. Bhatnagar et al. [52] showed a calibration framework based on a deep neural network with long short-term memory layers. Tian et al. [53] performed inference of model parameters based on reinforcement learning. See others in [54, 55]. However, these methods have limitations in predicting the reality when the number of observations is small and the calibrated models fit the experimental data poorly since the calibration parameters become unidentifiable [32]. To address this, the s-GaSP has modified the discrepancy function (i.e., the difference between the simulation model and experimental data) to obtain an emulator that more accurately approximates the real process response [32]. In this paper, we implemented the s-GaSP approach to efficiently calibrate the unknown parameters (i.e., density, viscosity, and surface tension) of specific printing scenarios with limited observations; hence, accurate droplets' volume predictions are possible in the IJP process.

TABLE 1: Process and Material Properties Ranges for the IJP Simulation Data Generation.

Variable	Range
Voltage (V)	[10, 50]
Surface Tension (N/m)	[0.02, 0.09]
Viscosity (cP)	[0.5, 2]
Density (g/ml)	[0.5, 1.2]

3. PROPOSED FRAMEWORK

3.1 Overview of the Proposed Framework

An illustration of the proposed framework is presented in Fig. 2. Figs. 2 (a)-(b) show the IJP simulation and experimental setups, respectively. Droplet images are collected from the simulated and experimental setups. Subsequently, image processing is deployed to calculate the volume of the jetted droplets, as shown in Fig. 2 (c). Different driving voltage regimes (i.e., voltage (V) range $[18, 38]$) were analyzed to obtain various droplet behaviors in the experimental setup, while distinct voltage regimes and material properties, i.e., density, viscosity, and surface tension (see Table 1), were explored in the simulation setup. n simulated and m experimental samples were collected for droplet volume emulator construction and subsequent calibration (see Figs. 2 (c)-(d)), correspondingly. After emulation and calibration, our framework is able to rapidly and accurately predict the IJP droplets' volume for unseen voltage regimes.

3.2 Experimental Setup

The hardware of the IJP experimental setup is shown in Fig. 2 (b). In this system, a piezo-based nozzle (MicroFab Inc.) is used as the inkjet print-head with typical Newtonian fluids to generate droplets. A CCD camera (Sensor Technologies Inc.) integrated with magnification lens works as the image-capturing device. In order to collect images of the droplet generation process, a strobing lighting technology, also known as synchronized illumination, is utilized to control the exposure time and obtain multi-image accumulation. It is assumed that the droplet shapes are axisymmetric to obtain the droplets' volume from the IJP images (see Fig. 2 (c)).

3.3 Simulated Setup

The NS equations govern the physical model mass and momentum conservation for the liquid-gas interface, and it is assumed that the fluid is viscous, axisymmetric, and incompressible. The mass conservation condition is established by,

$$\nabla \cdot \mathbf{u} = 0 \tag{1}$$

where $\mathbf{u}$ is the fluid velocity vector. Eq. (1) indicates that the amount of substance (ink) remains the same during the printing process. The momentum conservation, which is derived from the second Newton's law, is represented by,

$$\rho\left[\frac{\partial \mathbf{u}}{\partial t} + (\mathbf{u} \cdot \nabla)\mathbf{u}\right] = \nabla\sigma + f \tag{2}$$

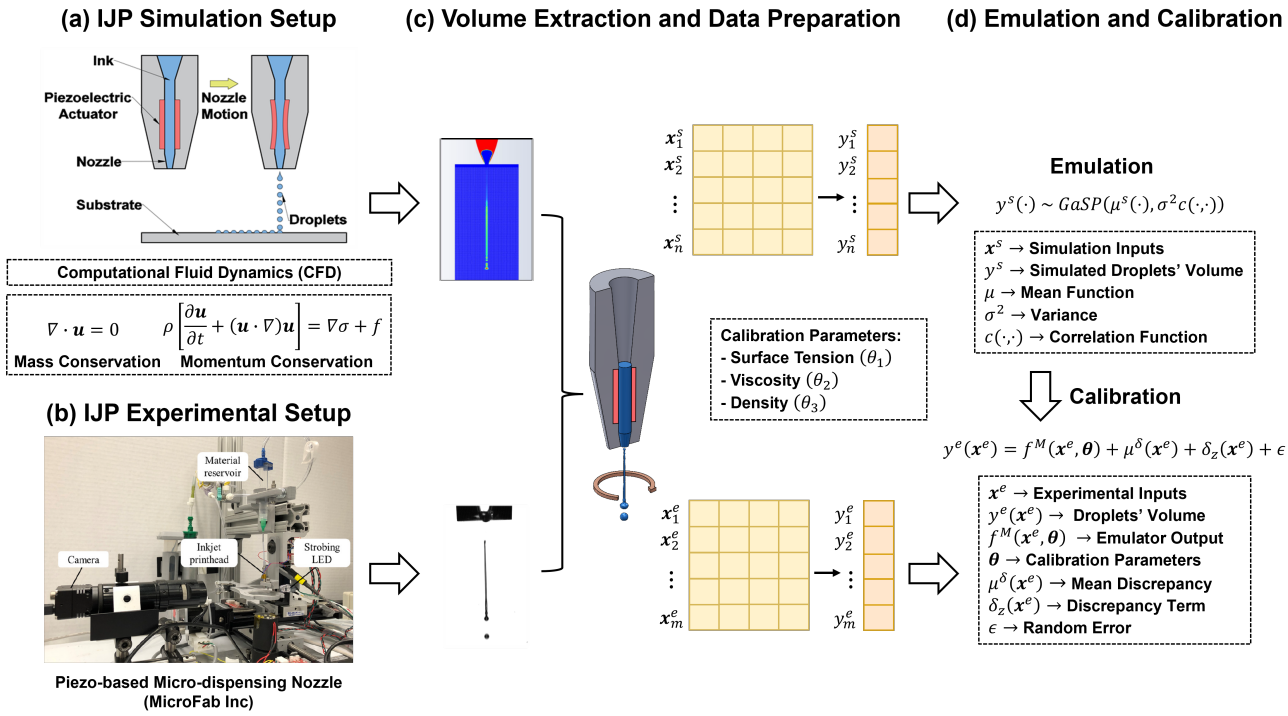

FIGURE 2: A Schematic Illustration of the Proposed Framework: (a) IJP Simulation Setup, (b) IJP Experimental Setup, (c) Volume Extraction and Data Preparation, and (d) Model Calibration.

where ρ is the density, $\left[\frac{\partial \mathbf{u}}{\partial t} + (\mathbf{u}\cdot\nabla)\mathbf{u}\right]$ is the acceleration component, and $\nabla\sigma + f$ is the total force that entails shear stress ($\nabla\sigma$) and other external forces (f). $\nabla\sigma$ can be divided into pressure-related and viscosity-related components, which are represented as $-\nabla p$ and $\mu\nabla^2\mathbf{u}$, respectively. The constitutive model that describes the inkjet droplet formation process is solved in ANSYS-Fluent. The volume-of-fluid (VOF) approach is utilized to track the droplet position and shape. In order to solve the pressure-velocity coupling problem, we use the fractional step scheme, the least squares cell-based gradient evaluation, the pressure staggering option scheme, and the QUICK scheme for quadrilateral and hexahedral meshes. The general mesh size used was $2 \times 10^{-5} m$. The geometry design was developed based on the assumption that the whole inkjet droplet generation process is axisymmetric; thus, we only defined half of the cross area of the geometry. The inner part of the printhead ink undergoes a wave propagation induced by the piezoelectric deformation. The piezoelectric action is determined by the applied voltage. The relation between the applied voltage and the piezoelectric actuator displacement can be approximated as a lineal relation, defined by $\Delta d_{radial} \approx d_{33} \cdot V$, where Δd_{radial} is the radial displacement, d_{33} is the piezoelectric coefficient and V is the voltage. See more details in [56].

Since ANSYS-Fluent permits to create materials with various physical property values (i.e., density, viscosity, surface tension, etc.), we explore several material properties of the most widely available ink materials for the simulation (see Table 1). Additionally, we used the Ohnesorge (Oh) number to define the jettability regime of the IJP process and explored the Oh number range between 0.0067 to 0.1579.

3.4 Scaled Gaussian Stochastic Process (s-GaSP)

Obtaining consistent droplet volume is crucial for the IJP process, and it is challenging to achieve. Having surrogate models that permit a wide range of materials and process parameters exploration is important to have a better process understanding that may derive in substantial quality improvements. The s-GaSP approach is able to efficiently support the construction of a calibrated surrogate model from simulated and experimental data, which will deliver fast and accurate predictions [32].

We first construct an emulator from the physics-based simulated IJP data. Let $\mathbf{x}_i^s \in \mathcal{X}$ the input variables (i.e., material and process parameters) that will influence the droplets' volumes $y_i^s \in \mathbb{R}$, $i = 1, ..., n$, and can be modeled as:

$$y^s(\cdot) \sim GaSP\left(\mu^s(\cdot), \sigma^2 c(\cdot,\cdot)\right), \tag{3}$$

where $\mu^s(\cdot)$ is the mean function and $\sigma^2 c(\cdot,\cdot)$ is the covariance function with variance σ^2 and correlation function $c(\cdot,\cdot)$. For any inputs $\mathbf{x}_i^s$, the outputs $\left(y^s(\mathbf{x}_1^s), ..., y^s(\mathbf{x}_n^s)\right)^T$ follow a multivariate normal distribution, $\left[\left(y^s(\mathbf{x}_1^s), ..., y^s(\mathbf{x}_n^s)\right)^T \middle| \mu^{\mathbf{S}}, \sigma^2, \mathbf{R}\right] \sim \mathcal{MN}\left(\left(\mu^s(\mathbf{x}_1^s), ..., \mu^s(\mathbf{x}_n^s)\right)^T, \sigma^2\mathbf{R}\right)$. $\mathbf{R}$ denotes the correlation matrix with the (i, j) entry $c(\mathbf{x}_i^s, \mathbf{x}_j^s)$. The mean function is defined as: $\mu^s(\mathbf{x}^s) = E^s\left[y^s(\mathbf{x}^s)\right] = \mathbf{h}^s(\mathbf{x}^s)\boldsymbol{\theta}^s = \sum_{t=1}^{q} h_t^s(\mathbf{x}^s)\theta_t^s$, here $\mathbf{h}^s(\mathbf{x}^s) = \left(h_1^s(\mathbf{x}^s), ..., h_q^s(\mathbf{x}^s)\right)$ is q-dimensional vector of basis functions and $\boldsymbol{\theta}^s = (\theta_1^s, ..., \theta_q^s)^T$ with θ_t^s being an unknown regression parameter for the basis function h_t^s. See [57] for details. The resulting emulator can make fast and accurate physics-based model IJP droplets' volume predictions for unseen material

and process parameters.

Since some parameters, such as density, viscosity, and surface tension, are unobservable in experiments (IJP experimental setup data), we need to calibrate the unknown parameters until the outputs of the emulator fit the experimental data. Let $\mathbf{x}_k^e$ be the inputs (i.e., IJP driving voltage) that will influence the experimental droplets' volume $y^e(\mathbf{x}_k^e)$, $k = 1, ..., m$. The computer model (i.e., emulator) outputs, defined as $f^M(\mathbf{x}_k^e, \boldsymbol{\theta})$, are evaluated at variable input $\mathbf{x}^e \in \mathcal{X}^e$ and calibration parameter $\boldsymbol{\theta}$. The s-GasP statistical model calibration is defined as [32]:

$$y^e(\mathbf{x}^e) = f^M(\mathbf{x}^e, \boldsymbol{\theta}) + \mu^\delta(\mathbf{x}^e) + \delta_z(\mathbf{x}^e) + \epsilon, \tag{4}$$

where $\delta_z(\mathbf{x}^e) = \left\{\delta(\mathbf{x}^e) \middle| \int_{\xi \in \mathfrak{X}^e} \delta(\boldsymbol{\xi})^2 d\boldsymbol{\xi} = Z\right\}$, $\delta(\cdot) \sim GaSP\left(0, \sigma_\delta^2 c^\delta(\cdot,\cdot)\right)$, $\epsilon \sim N(0, \sigma_0^2)$. In particular, given $Z = z$, the new process $\delta_z(\cdot)$ is a GaSP $\delta(\cdot)$ constrained at the space of $\int_{\xi \in \mathfrak{X}^e} \delta(\boldsymbol{\xi})^2 d\boldsymbol{\xi} = z$ [32]. $\mu^\delta(\mathbf{x}^e) = \mathbf{h}^\delta(\mathbf{x}^e)\boldsymbol{\beta}^\delta = \sum_{l=1}^{q_\delta} h_l^\delta(\mathbf{x}^e)\beta_l^\delta$ is the mean discrepancy, which is modeled by regression. Here, $\boldsymbol{h}^\delta$ is a known q_δ-dimensional vector of basis functions and β^δ is an unknown q_δ-dimensional vector with each β_l^δ being the regression parameter of $h_l^\delta(\mathbf{x}^e)$ for $l = 1, ..., q_\delta$.

The marginal distribution of discrepancy $\boldsymbol{\delta}_z = \left(\delta_z(\mathbf{x}_1^e), ..., \mathbf{x}_k^e)\right)^T$ is a multivariate normal distribution:

$$\boldsymbol{\delta}_z | \boldsymbol{\Theta} \sim \mathcal{MN}\left(\mathbf{0}, \sigma_\delta^2 \mathbf{R}_z\right) \tag{5}$$

where $\boldsymbol{\Theta}$ denotes the model parameters and $\mathbf{R}_z$ is the covariance function $\mathbf{R}_z = \left(\mathbf{B} + \left(\mathbf{R}^\delta\right)^{-1}\right)^{-1}$. Here, $\mathbf{B}$ is an $n \times n$ real-valued matrix and $\mathbf{R}^\delta$ is a correlation matrix such that its (i, j) entry is defined as $R_{i,j}^\delta = c^\delta(\mathbf{x}_i^e, \mathbf{x}_j^e)$. The power exponential correlation is defined as: $c_l^\delta(d_l) = exp\left\{-\left(\frac{d_l}{\gamma_l^\delta}\right)^{v_l^\delta}\right\}$. $d_l = |x_{al} - x_{bl}|$ is the distance of the l^{th} coordinate of the input vectors. v_l^δ is a roughness parameter typically held fixed and γ_l^δ is an unknown range parameter to be estimated. The Matérn correlation with the roughness parameter is $v_l^\delta = \frac{(2t+1)}{2}$ for $t \in \mathbb{N}$ has a closed-form expression, and can be seen in [32]. The model parameters $\boldsymbol{\Theta} = \left[\boldsymbol{\theta}, \beta^\delta, \gamma^\delta, \sigma_\delta^2, \sigma_0^2\right]$ are obtained through the Markov Chain Monte Carlo (MCMC) sampling from the posterior distribution [57]

$$p\left(\boldsymbol{\Theta} | \mathbf{y}^e\right) \propto p\left(\boldsymbol{\Theta}\right) p\left(\mathbf{y}^e | \boldsymbol{\Theta}\right) \tag{6}$$

where $p\left(\boldsymbol{\Theta}\right)$ is the prior distribution of the unknown parameters and it is assumed to be uniform over the parameters space. Closed-form expressions of the posterior distribution and MCMC algorithm are provided in [32, 57, 58]. After obtaining the posterior distribution, one can predict the $\hat{y}_{new}^e\left(\mathbf{x}_{new}^e\right)$ at new process setting $\mathbf{x}_{new}^e$.

4. CASE STUDY

As mentioned in the Introduction, droplet volume consistency is crucial for the quality preservation of printed parts in the IJP process. Having a rapid and accurate mechanism to make volume predictions will help to obtain consistent droplet volume during the process. In this section, we demonstrate that after

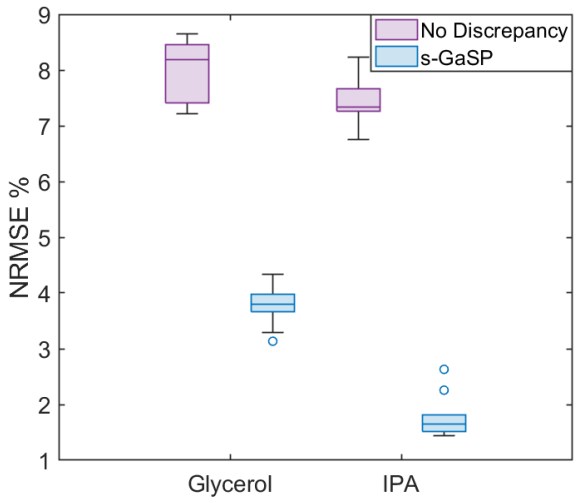

FIGURE 3: FFCV NRMSE for the No Discrepancy and s-GaSP Discrepancy Models Using the Two Distinct Materials (Glycerol and IPA).

unknown material parameters (i.e., density, viscosity, and surface tension) calibration, the proposed framework makes fast and accurate droplet volume predictions.

The simulated data are obtained by solving the mass and momentum conservation equations as presented in 3.3. The simulations are run by setting 4 cores, time step size equals $9 \times 10^{-8} s$, 1200 time steps, contact angle of 90°, and nozzle diameter of 50 μm. To systematically investigate the impact of the input factors, a Latin hypercube sampling design is established. Different material (e.g., density and viscosity) and process (e.g., driving voltage) parameters are explored. 20 simulation samples are used to show the performance of the model using limited data. For the experimental measurements, we analyzed two ink materials (20% glycerol solution and isopropyl alcohol (IPA)). Here, both

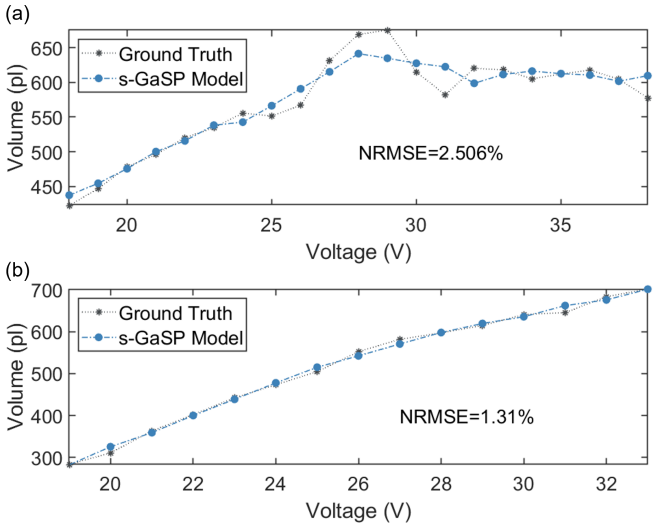

FIGURE 4: LOOCV Results of the Droplet Volume Prediction Based on the Voltage Applied for Two Materials: (a) Glycerol, and (b) IPA.

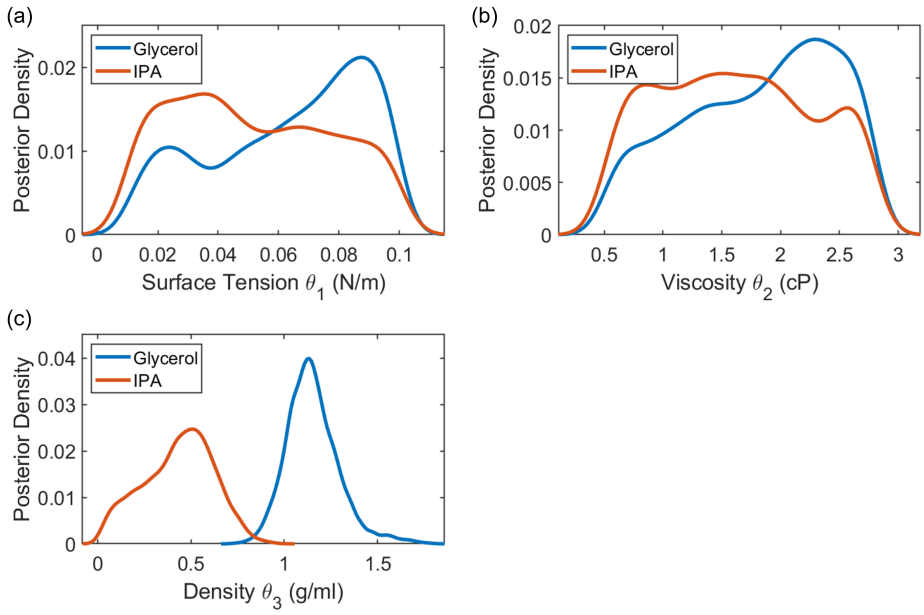

FIGURE 5: Posterior Value Densities of the Calibration Parameters (i.e., Ink Properties) for Glycerol (Blue) and IPA (Orange) Materials: (a) Surface Tension, (b) Viscosity, and (c) Density.

experimental fluids are considered to have a Newtonian behavior. We obtain 21 and 15 samples of glycerol and IPA, respectively, for the analysis. The ink materials are jetted with a piezo-driven dispenser of 40 μm nozzle diameter. The proposed framework is run in a computer with an AMD Ryzen 7 4800H CPU @ 2.89 GHz, and 16.0 GB.

To evaluate the overall performance of the proposed framework, we perform five-fold cross validation (FFCV) with 10 replications for each material, where the normalized root mean squared error (NRMSE) is obtained by using NRMSE $= \frac{\|y^e - \hat{y}^e\|}{\|y^e\|}$. y^e is the ground truth droplet volume, and $\hat{y}^e$ is the predicted droplet volume. The FFCV evaluation is performed with two variations of the calibration model. First, we try a model without the discrepancy function (i.e., the experimental data is modeled with the emulation response and the measurement error) and a model including the discrepancy function (s-GaSP). Fig. 3 illustrates the error obtained in each iteration of the FFCV for the No Discrepancy (purple) and s-GaSP discrepancy (blue) models using the two distinct materials (glycerol and IPA). From Fig. 3, the NRMSE is reduced when integrating the s-GaSP discrepancy function in the calibration model. In particular, this is more evident in the IPA material. Fig. 3 suggests that the s-GaSP calibration model produces low-variability errors for both ink materials, which implies more consistent predictions. In addition, the modeling and prediction time is captured for the s-GaSP calibration. The average computational time for emulation and calibration is 2.8162 seconds, meanwhile, the average computation time for prediction was 0.4448 seconds. Based on the average modeling and prediction times, the proposed framework response is much faster than CFD model simulations.

Furthermore, we implement leave-one-out cross validation (LOOCV) to obtain a robust estimation of the model's performance and to evaluate the model's sensibility using a single test set. The results of the LOOCV for glycerol and IPA are shown in Fig. 4 (a)-(b), respectively. The measured droplet volume (ground truth) (gray) and the model prediction (blue) for various input voltage values are presented. One can see that the highest NRMSE is obtained using glycerol (2.506%). This could happen because of the high non-linearity of the droplet volume. However, model prediction accuracy is acceptable because the model performs reliable estimations of the droplet volume for both materials.

The marginal posterior densities of the calibration parameters (i.e., ink properties) for glycerol and IPA are obtained by the posterior samples in the MCMC algorithm. The distribution for the surface tension, viscosity, and density are displayed in Figs. 5 (a)-(c), respectively. Fig. 5 (a) suggests a surface tension for the glycerol solution around 0.08 N/m, which is close to the experimental measurement (0.07093 N/m at 20 $^\circ C$). Similarly, the IPA's surface tension is around 0.04 N/m, approaching the experimental value (0.02179 N/m at 15 $^\circ C$). The posterior mass of the viscosity spreads widely throughout its domain for both materials, see Fig. 5 (b). The uncertainties of the viscosity seem quite large, for both materials, given that it depends on environmental conditions. From Fig. 5 (c), the posterior median of the ink's density for glycerol is around 1.15 g/ml, meanwhile, the experimental measurement is 1.05 g/ml at 20 $^\circ C$. Moreover, the IPA's density posterior median is 0.6 g/ml, which comes near 0.77 g/ml (i.e., the experimental measurement). Thus, both calibrated density values are close to the physical property value of each analyzed material.

Concisely, the proposed model calibration framework can accurately and efficiently predict the droplet volume and can estimate the unknown parameters in the IJP process. The proposed

framework can be applied to a broad range of ink/solution materials and other complex-behavior processes.

5. CONCLUSION

IJP is able to produce multi-material parts with high resolution for an extensive variety of application fields, which require droplets' volume consistency. However, the droplets' volume depends critically on fluid and process parameters. Predicting the droplet volume, based on the input parameters, is predominant but has been difficult since some IJP's parameters are unknown. In this paper, we propose a framework that is capable to calibrate the unknown process parameters and fulfilling fast and accurate droplet volume predictions via s-GaSP modeling. The proposed calibration framework can be applied to other AM processes with limited data and complex dynamics.

In the future, we will extend this framework by integrating multiple source auxiliary observations so that it can identify the measurement bias and model discrepancy for the IJP process, and provide better estimates of unknown parameters. Another research direction that can be explored is the calibration of the IJP process using nanoparticles-based inks since the nanoparticles affect the ink physical properties; and, this lead to modification in the droplet size, shape, and volume.

ACKNOWLEDGMENTS

This work is partially supported by the NSF Grant No. FM-2134409, Jon Rieger Seed Grant at the University of Louisville, and KY NSF EPSCoR Emerging Research Ideas (ERI) Program.

REFERENCES

[1] Charles, Amal, Elkaseer, Ahmed, Thijs, Lore, Hagenmeyer, Veit and Scholz, Steffen. "Effect of process parameters on the generated surface roughness of down-facing surfaces in selective laser melting." *Applied Sciences* Vol. 9 No. 6 (2019): p. 1256.

[2] Das, Paramita, Chandran, Ramya, Samant, Rutuja and Anand, Sam. "Optimum part build orientation in additive manufacturing for minimizing part errors and support structures." *Procedia Manufacturing* Vol. 1 (2015): pp. 343–354.

[3] Yuan, Jiangping, Chen, Chen, Yao, Danyang and Chen, Guangxue. "3D printing of oil paintings based on material jetting and its reduction of staircase effect." *Polymers* Vol. 12 No. 11 (2020): p. 2536.

[4] Kowsari, Kavin, Zhang, Biao, Panjwani, Sahil, Chen, Zaichun, Hingorani, Hardik, Akbari, Saeed, Fang, Nicholas X and Ge, Qi. "Photopolymer formulation to minimize feature size, surface roughness, and stair-stepping in digital light processing-based three-dimensional printing." *Additive Manufacturing* Vol. 24 (2018): pp. 627–638.

[5] Bhole, Kiran, Ekshinge, Sunil and Gandhi, Prasanna. "Fabrication of continuously varying thickness micro-cantilever using bulk lithography process." *International Manufacturing Science and Engineering Conference*, Vol. 45806: p. V001T01A009. 2014. American Society of Mechanical Engineers.

[6] Nayak, Laxmidhar, Mohanty, Smita, Nayak, Sanjay Kumar and Ramadoss, Ananthakumar. "A review on inkjet printing of nanoparticle inks for flexible electronics." *Journal of Materials Chemistry C* Vol. 7 No. 29 (2019): pp. 8771–8795.

[7] Mauthner, Gernot, Landfester, Katharina, Köck, Anton, Brückl, Hubert, Kast, Michael, Stepper, Christoph and List, Emil JW. "Inkjet printed surface cell light-emitting devices from a water-based polymer dispersion." *Organic Electronics* Vol. 9 No. 2 (2008): pp. 164–170.

[8] Zaugg, Frank G and Wagner, Peter. "Drop-on-demand printing of protein biochip arrays." *Mrs Bulletin* Vol. 28 No. 11 (2003): pp. 837–842.

[9] Saunders, Rachel Elizabeth and Derby, Brian. "Inkjet printing biomaterials for tissue engineering: bioprinting." *International Materials Reviews* Vol. 59 No. 8 (2014): pp. 430–448.

[10] Singh, Madhusudan, Haverinen, Hanna M, Dhagat, Parul and Jabbour, Ghassan E. "Inkjet printing—process and its applications." *Advanced materials* Vol. 22 No. 6 (2010): pp. 673–685.

[11] Herran, C Leigh, Huang, Yong and Chai, Wenxuan. "Performance evaluation of bipolar and tripolar excitations during nozzle-jetting-based alginate microsphere fabrication." *Journal of micromechanics and microengineering* Vol. 22 No. 8 (2012): p. 085025.

[12] Hoath, Stephen D. *Fundamentals of inkjet printing: the science of inkjet and droplets*. John Wiley & Sons (2016).

[13] Brünahl, Jürgen and Grishin, Alex M. "Piezoelectric shear mode drop-on-demand inkjet actuator." *Sensors and Actuators A: Physical* Vol. 101 No. 3 (2002): pp. 371–382.

[14] Pesach, Dora and Marmur, Abraham. "Marangoni effects in the spreading of liquid mixtures on a solid." *Langmuir* Vol. 3 No. 4 (1987): pp. 519–524.

[15] Eggers, Jens. "Nonlinear dynamics and breakup of free-surface flows." *Reviews of modern physics* Vol. 69 No. 3 (1997): p. 865.

[16] Elkaseer, Ahmed, Schneider, Stella, Deng, Yaqi and Scholz, Steffen G. "Effect of process parameters on the performance of drop-on-demand 3D inkjet printing: Geometrical-based modeling and experimental validation." *Polymers* Vol. 14 No. 13 (2022): p. 2557.

[17] Rahul, SH, Balasubramanian, K and Venkatesh, Sriram. "Optimizing inkjet printing process to fabricate thick ceramic coatings." *Ceramics International* Vol. 43 No. 5 (2017): pp. 4513–4519.

[18] Gheno, Alexandre, Huang, Yong, Bouclé, Johann, Ratier, Bernard, Rolland, Alain, Even, Jacky and Vedraine, Sylvain. "Toward highly efficient inkjet-printed perovskite solar cells fully processed under ambient conditions and at low temperature." *Solar RRL* Vol. 2 No. 11 (2018): p. 1800191.

[19] Le, Minh Quyen, Ganet, Florent, Audigier, David, Capsal, Jean-Fabien and Cottinet, Pierre-Jean. "Printing of microstructure strain sensor for structural health monitoring." *Applied Physics A* Vol. 123 No. 5 (2017): pp. 1–9.

[20] Shin, Pyungho, Sung, Jaeyong and Lee, Myeong Ho. "Control of droplet formation for low viscosity fluid by double

waveforms applied to a piezoelectric inkjet nozzle." *Microelectronics Reliability* Vol. 51 No. 4 (2011): pp. 797–804.

[21] Huang, Jida, Segura, Luis Javier, Wang, Tianjiao, Zhao, Guanglei, Sun, Hongyue and Zhou, Chi. "Unsupervised learning for the droplet evolution prediction and process dynamics understanding in inkjet printing." *Additive Manufacturing* Vol. 35 (2020): p. 101197.

[22] Cao, Xianghong, Ye, Yun, Tang, Qian, Chen, Enguo, Jiang, Zongzhao, Pan, Jianhao and Guo, Tailiang. "Numerical analysis of droplets from multinozzle inkjet printing." *The Journal of Physical Chemistry Letters* Vol. 11 No. 19 (2020): pp. 8442–8450.

[23] Rembe, Christian, aus der Wiesche, Stefan, Beuten, Michael and Hofer, Eberhard P. "Nonreproducible phenomena in thermal ink jets with real high-speed cine photomicrography." *Electronic Imaging: Processing, Printing, and Publishing in Color*, Vol. 3409: pp. 316–325. 1998. SPIE.

[24] Tsai, Ming-Hsiu and Hwang, Weng-Sing. "Effects of pulse voltage on the droplet formation of alcohol and ethylene glycol in a piezoelectric inkjet printing process with bipolar pulse." *Materials transactions* Vol. 49 No. 2 (2008): pp. 331–338.

[25] Wu, Dazhong and Xu, Changxue. "Predictive modeling of droplet formation processes in inkjet-based bioprinting." *Journal of Manufacturing Science and Engineering* Vol. 140 No. 10 (2018).

[26] Laurila, MM, Khorramdel, B, Dastpak, A and Mäntysalo, M. "Statistical analysis of E-jet print parameter effects on Ag-nanoparticle ink droplet size." *Journal of Micromechanics and Microengineering* Vol. 27 No. 9 (2017): p. 095005.

[27] Hu, Shaowei, Zhu, Wenbo, Yang, Wanchun and Li, Mingyu. "Morphology simulation of drop-on-demand inkjet-printed droplets." *npj Flexible Electronics* Vol. 6 No. 1 (2022): pp. 1–11.

[28] Wu, Hsuan-Chung, Lin, Huey-Jiuan, Kuo, Yung-Chi and Hwang, Weng-Sing. "Simulation of droplet ejection for a piezoelectric inkjet printing device." *Materials Transactions* Vol. 45 No. 3 (2004): pp. 893–899.

[29] Siregar, DP, Kuerten, Johannes GM and Van Der Geld, CWM. "Numerical simulation of the drying of inkjet-printed droplets." *Journal of colloid and interface science* Vol. 392 (2013): pp. 388–395.

[30] Kennedy, Marc C and O'Hagan, Anthony. "Bayesian calibration of computer models." *Journal of the Royal Statistical Society: Series B (Statistical Methodology)* Vol. 63 No. 3 (2001): pp. 425–464.

[31] Tuo, Rui and Wu, CF Jeff. "Efficient calibration for imperfect computer models." *The Annals of Statistics* Vol. 43 No. 6 (2015): pp. 2331–2352.

[32] Gu, Mengyang and Wang, Long. "Scaled Gaussian stochastic process for computer model calibration and prediction." *SIAM/ASA Journal on Uncertainty Quantification* Vol. 6 No. 4 (2018): pp. 1555–1583.

[33] Corzo, Daniel, Almasabi, Khulud, Bihar, Eloise, Macphee, Sky, Rosas-Villalva, Diego, Gasparini, Nicola, Inal, Sahika and Baran, Derya. "Digital inkjet printing of high-efficiency large-area nonfullerene organic solar cells." *Advanced Materials Technologies* Vol. 4 No. 7 (2019): p. 1900040.

[34] Andò, Bruno, Baglio, Salvatore, Bulsara, Adi R, Emery, Teresa, Marletta, Vincenzo and Pistorio, Antonio. "Low-cost inkjet printing technology for the rapid prototyping of transducers." *Sensors* Vol. 17 No. 4 (2017): p. 748.

[35] Castrejon-Pita, Jose Rafael, Baxter, WRS, Morgan, J, Temple, S, Martin, GD and Hutchings, Ian M. "Future, opportunities and challenges of inkjet technologies." *Atomization and sprays* Vol. 23 No. 6 (2013).

[36] Khan, Arshad, Roo, Joan Sol, Kraus, Tobias and Steimle, Jürgen. "Soft inkjet circuits: rapid multi-material fabrication of soft circuits using a commodity inkjet printer." *Proceedings of the 32nd Annual ACM Symposium on User Interface Software and Technology*: pp. 341–354. 2019.

[37] Zhang, Yanzhen, Li, Dege, Liu, Yonghong and Wittstock, Gunther. "Inkjet printing in liquid environments." *Small* Vol. 14 No. 27 (2018): p. 1801212.

[38] Castrejón-Pita, JR, Martin, GD, Hoath, SD and Hutchings, IM. "A simple large-scale droplet generator for studies of inkjet printing." *Review of Scientific Instruments* Vol. 79 No. 7 (2008): p. 075108.

[39] Tai, Jiayan, Gan, Hiong Yap, Liang, Yen Nan and Lok, Boon Keng. "Control of droplet formation in inkjet printing using Ohnesorge number category: Materials and processes." *2008 10th Electronics Packaging Technology Conference*: pp. 761–766. 2008. IEEE.

[40] Ball, Amit Kumar, Das, Raju, Roy, Shibendu Shekhar, Kisku, Dakshina Ranjan and Murmu, Naresh Chandra. "Modeling of EHD inkjet printing performance using soft computing-based approaches." *Soft Computing* Vol. 24 No. 1 (2020): pp. 571–589.

[41] Segura, Luis Javier, Wang, Tianjiao, Zhou, Chi and Sun, Hongyue. "Online droplet anomaly detection from streaming videos in inkjet printing." *Additive Manufacturing* Vol. 38 (2021): p. 101835.

[42] Tourloukis, Georgios, Stoyanov, Stoyan, Tilford, Tim and Bailey, Chris. "Data driven approach to quality assessment of 3D printed electronic products." *2015 38th International Spring Seminar on Electronics Technology (ISSE)*: pp. 300–305. 2015. IEEE.

[43] Ramakrishnan, N, Rajesh, PK, Ponnambalam, P and Prakasan, K. "Studies on preparation of ceramic inks and simulation of drop formation and spread in direct ceramic inkjet printing." *Journal of Materials Processing Technology* Vol. 169 No. 3 (2005): pp. 372–381.

[44] Park, Yubin, Park, Yeseul, Lee, Jiwon and Lee, Changhee. "Simulation for forming uniform inkjet-printed quantum dot layer." *Journal of Applied Physics* Vol. 125 No. 6 (2019): p. 065304.

[45] He, Bing, Yang, Sucui, Qin, Zhangrong, Wen, Binghai and Zhang, Chaoying. "The roles of wettability and surface tension in droplet formation during inkjet printing." *Scientific reports* Vol. 7 No. 1 (2017): pp. 1–7.

[46] Jiang, Liangkui, Yu, Li, Premaratne, Pavithra, Zhang, Zhan and Qin, Hantang. "CFD-based numerical modeling to pre-

dict the dimensions of printed droplets in electrohydrodynamic inkjet printing." *Journal of Manufacturing Processes* Vol. 66 (2021): pp. 125–132.

[47] Santner, Thomas J, Williams, Brian J, Notz, William I and Williams, Brain J. *The design and analysis of computer experiments*. Vol. 1. Springer (2003).

[48] Segura, Luis Javier, Zhao, Guanglei, Zhou, Chi and Sun, Hongyue. "Nearest neighbor gaussian process emulation for multi-dimensional array responses in freeze nano 3d printing of energy devices." *Journal of Computing and Information Science in Engineering* Vol. 20 No. 4 (2020).

[49] Sargsyan, K, Najm, HN and Ghanem, R. "On the statistical calibration of physical models." *International Journal of Chemical Kinetics* Vol. 47 No. 4 (2015): pp. 246–276.

[50] Sun, Hongyue, Luo, Shuai, Jin, Ran and He, Zhen. "Ensemble engineering and statistical modeling for parameter calibration towards optimal design of microbial fuel cells." *Journal of Power Sources* Vol. 356 (2017): pp. 288–298.

[51] Mahmoudi, Mohamad, Tapia, Gustavo, Karayagiz, Kubra, Franco, Brian, Ma, Ji, Arroyave, Raymundo, Karaman, Ibrahim and Elwany, Alaa. "Multivariate calibration and experimental validation of a 3D finite element thermal model for laser powder bed fusion metal additive manufacturing." *Integrating Materials and Manufacturing Innovation* Vol. 7 No. 3 (2018): pp. 116–135.

[52] Bhatnagar, Saumya, Chang, Won, Kim, Seonjin and Wang, Jiali. "Computer Model Calibration with Time Series Data Using Deep Learning and Quantile Regression." *SIAM/ASA Journal on Uncertainty Quantification* Vol. 10 No. 1 (2022): pp. 1–26.

[53] Tian, Yuan, Chao, Manuel Arias, Kulkarni, Chetan, Goebel, Kai and Fink, Olga. "Real-time model calibration with deep reinforcement learning." *Mechanical Systems and Signal Processing* Vol. 165 (2022): p. 108284.

[54] Meißner, Paul, Watschke, Hagen, Winter, Jens and Vietor, Thomas. "Artificial neural networks-based material parameter identification for numerical simulations of additively manufactured parts by material extrusion." *Polymers* Vol. 12 No. 12 (2020): p. 2949.

[55] Greve, CM, Hara, K, Martin, RS, Eckhardt, DQ and Koo, JW. "A data-driven approach to model calibration for nonlinear dynamical systems." *Journal of Applied physics* Vol. 125 No. 24 (2019): p. 244901.

[56] Wang, Tianjiao. "Inkjet 3D Printing Process Monitoring and Control for Quality Improvement." Ph.D. Thesis, State University of New York at Buffalo. 2021.

[57] Gu, Mengyang, Wang, Xiaojing and Berger, James O. "Robust Gaussian stochastic process emulation." *The Annals of Statistics* Vol. 46 No. 6A (2018): pp. 3038–3066.

[58] Gu, Mengyang. "RobustCalibration: Robust Calibration of Computer Models in R." *arXiv preprint arXiv:2201.01476* (2022).